Journal of Cerebral Blood Flow & Metabolism (2013) 33, 1279–1285

www.jcbfm.com

ORIGINAL ARTICLE

Longitudinal effects of lesions on functional networks after stroke

Smadar Ovadia-Caro[1,2,3], Kersten Villringer[4], Jochen Fiebach[4], Gerhard Jan Jungehulsing[4,5], Elke van der Meer[1,3], Daniel S Margulies[1,2] and Arno Villringer[1,2,4]

While ischemic stroke reflects focal damage determined by the affected vascular territory, clinical symptoms are often more complex and may be better explained by additional indirect effects of the focal lesion. Assumed to be structurally underpinned by anatomical connections, supporting evidence has been found using alterations in the functional connectivity of resting-state functional magnetic resonance imaging (fMRI) data in both sensorimotor and attention networks. To assess the generalizability of this phenomenon in a stroke population with heterogeneous lesions, we investigated the distal effects of lesions on a global level. Longitudinal resting-state fMRI scans were acquired at three consecutive time points, beginning during the acute phase (days 1, 7, and 90 post-stroke) in 12 patients after ischemic stroke. We found a preferential functional change in affected networks (i.e., networks containing lesions changed more during recovery when compared with unaffected networks). This change in connectivity was significantly correlated with clinical changes assessed with the National Institute of Health Stroke Scale. Our results provide evidence that the functional architecture of large-scale networks is critical to understanding the clinical effect and trajectory of post-stroke recovery.

Journal of Cerebral Blood Flow & Metabolism (2013) **33,** 1279–1285; doi:10.1038/jcbfm.2013.80; published online 29 May 2013

Keywords: concordance; dual regression; heterogeneous lesions; intrinsic functional connectivity; resting-state fMRI

INTRODUCTION

The brain is a complex network of interacting functionally and structurally connected regions. As brain functions emerge from interacting regions that are part of a network topology,[1–4] so too can alterations across networks coincide with various pathological states such as disorders of consciousness,[5,6] Alzheimer's disease,[7] neuropsychiatric disorders,[8] and stroke.[9–13] Stroke lesions provide a unique model of how local damage can result in long-distance alterations. Similar structural damage has been shown to result in different levels of impairment to functionality, and patients can present multiple deficits in the acute phase that are not easily attributed to the direct effect of the focal lesion.[10,14] The complex symptoms not explained by damage to the infarct core are partially explained by hypoperfusion in penumbral areas surrounding the lesion,[15,16] as well as effects on distal regions connected to the damaged tissue.[17]

Using functional connectivity measures based on temporal correlation of spontaneous blood oxygenation level-dependent (BOLD) signal fluctuations (resting-state fMRI), it has previously been shown that localized brain lesions can cause connectivity-based changes in regions that are structurally intact and far from the lesion site. This phenomenon has been demonstrated in the motor[13,18,19] and attention networks,[9,20] and has also been shown to correlate with behavioral improvement in the post-stroke recovery phase.[9,13,18–20]

Heterogeneity of lesions in terms of location and size is one of the notorious challenges in stroke research. A generalizable analytic method could enable investigators to explore changes within several networks to address a single question. In a recent study by Nomura *et al*[11] dissociation between two networks has been demonstrated in a group of chronic stroke patients with heterogeneous lesions. In their work, functional connectivity between and within two cognitive control networks (fronto-parietal and cingulo-opercular) was compared in patients with heterogeneous lesions affecting one network more than the other. They found decreased functional connectivity within the damaged, more than the undamaged, networks. Building on this line of research, our aims in the current study were to investigate whether this dissociation is generalizable, extending to all large-scale networks and to explore the feasibility of a global, whole-brain approach that can account for heterogeneous lesions across patients. Based on previously published empirical data[9,13,18–20] and computational models of stroke,[21,22] we hypothesized that lesions will result in larger alterations in functional connectivity over time in affected versus unaffected networks, demonstrating the generalizability of this phenomenon.

Here, we present a novel, network-based approach to study the longitudinal effects of heterogeneous lesions on functional networks. We apply whole-brain spatial concordance as a measure of change in the connectivity over time (as initially described in Lohmann *et al*[23]), and find that concordance preferentially decreases in affected networks across a heterogeneous lesion population. This finding reflects the general influence of localized lesions on distant functionally connected regions, and demonstrates the feasibility and potential of the suggested analytic approach for investigating resting-state fMRI data in a heterogeneous stroke population.

[1]Berlin School of Mind and Brain, The Mind-Brain Institute, Humboldt University, Berlin, Germany; [2]Max Planck Institute for Human Cognitive and Brain Sciences, Leipzig, Germany; [3]Institute of Psychology, Humboldt University, Berlin, Germany; [4]Center for Stroke Research, Charité University, Berlin, Germany and [5]Department of Neurology, Charité University, Berlin, Germany. Correspondence: S Ovadia-Caro, MSc, Berlin School of Mind and Brain, Humboldt-Universität zu Berlin, Luisenstraße 56, Haus 1, 10117 Berlin, Germany or Dr DS Margulies, Max Planck Institute for Human Cognitive and Brain Sciences, StephanStraße 1A, 04103 Leipzig, Germany.
E-mail: smadar.ovadia@gmail.com or margulies@cbs.mpg.de
Sources of support: The study was funded by Minerva Stiftung, DFG (Berlin School of Mind and Brain), Einstein Foundation Berlin (The Mind-Brain Institute), BMBF (Center for Stroke Research Berlin), and the German Competence Net Stroke.
Received 27 November 2012; revised 19 March 2013; accepted 26 April 2013; published online 29 May 2013

MATERIALS AND METHODS

Subjects

Thirty-one patients diagnosed with ischemic stroke were initially recruited for the study as part of the *1000+ Study* (registered in http://www.clinicaltrials.org, NCT00715533).[24] Inclusion criteria were first ever ischemic stroke within 24 hours, which was evident in imaging, and a minimum of three consecutive resting-state fMRI scans. Twelve patients were included in the current analysis due to exclusion criteria, including: antecedent lesions (5 excluded), brainstem or cerebellar infarcts, extensive white matter lesions defined as Wahlund score[25] $\geqslant 6$ (8 excluded), other brain abnormalities, revealed in anatomical scans (2 excluded), and less than three resting-state scans (4 patients), leaving 12 patients (age 64.25 ± 12.0 years, 8 males, 4 females) for the analysis. This study was approved by the ethics committee of the Charité-Universitätsmedizin, Berlin, Germany. Written informed consent was obtained from all patients.

Functional Imaging

Functional magnetic resonance imaging (fMRI) data were obtained during a 5.75-minutes (150 volumes) resting-state scan (i.e., spontaneous blood oxygenation level-dependent fluctuations) using a Siemens Tim Trio 3T scanner (Siemens Ag, Erlangen, Germany) at the Center for Stroke Research at the Charité University Hospital in Berlin. Patients were scanned at three consecutive time points after the stroke: day 1 post-stroke (1 day $\pm$ 0, mean $\pm$ std), day 7 post-stroke (8.25 ± 6.34 days), and day 90 post-stroke (90.12 ± 5.0 days). Day 1 was defined as the interval between 24 and 48 hours post-symptoms onset. The early acquisition was facilitated by the proximity of the scanner to the stroke unit. Two-dimensional functional images using blood oxygenation level-dependent contrast were obtained with an EPI sequence (TR = 2300 milliseconds, TE = 30 milliseconds, 30 slices, voxel size: 3.125 mm $\times$ 3.125 mm $\times$ 4 mm, flip angle 90°). T1-weighted anatomical images were acquired using a 3D MPRAGE sequence (TR = 1900 milliseconds, TE = 2.52 milliseconds, TI = 900 milliseconds, 192 slices, voxel size: 1 mm $\times$ 1 mm $\times$ 1 mm, flip angle 9°). Diffusion weighted images (DWI) and fluid attenuated inversion recovery (FLAIR) images acquired at day 1 post-stroke were used for lesion localization (in one patient, for which this data were not available for day 1 post-stroke, data from day 7 post-stroke were used). For further details on patients and scanning time points, see Supplementary Table S1.

fMRI Preprocessing

fMRI data were preprocessed using FSL (FMRIB Software Library, http://www.fmrib.ox.ac.uk) and AFNI (Analysis of Functional NeuroImages, http://afni.nimh.nih.gov/afni) software, based on the 1000 Functional Connectomes scripts (http://fcon_1000.projects.nitrc.org/). The first two images of each functional scan were discarded to avoid T1 saturation effects. Preprocessing of functional scans included: slice-time correction, 3D motion correction, spatial smoothing with a 6 mm full-width-at-half-maximum Gaussian kernel, band-pass filtering (0.009 to 0.1 Hz), removal of linear and quadratic trends and mean-based intensity normalization of all volumes by the same factor (10,000). Several sources of spurious variance were removed from the signal time-course of each voxel using the general linear model: global signal (average signal over the whole-brain mask), white matter signal, signal from the ventricles, and the six motion parameters. Mean motion displacement and rotation were computed for each patient and for each scan as described in Van Dijk *et al*.[26] Mean motion did not exceed a maximum of 2.5 mm in mean total displacement and 2.5 degrees in mean total rotation in any of the scans. For further details on patients' motion see Supplementary Table S2. We have made the scripts publically available: (https://github.com/NeuroanatomyAndConnectivity/checkMotion). To verify that global signal removal had not influenced the results, we repeated our analysis without this preprocessing step, and observed similar results (for further details, see Supplementary Material M1 and Supplementary Figure S1). Data were then normalized to the Montreal Neurologic Institute MNI152 template with 3 mm^3 resolution using FMRIB's Linear Image Registration Tool.[27,28] Each high-resolution structural image was registered to the MNI152 template by computing a 12 degrees-of-freedom linear affine transformation. Registration of each corresponding functional data to the high-resolution structural image was carried out using a linear transformation with 6 degrees-of-freedom. The structural-to-standard nonlinear transformation matrices were then applied to obtain a functional volume in MNI152 standard space.

Lesion Definition

Lesions were defined based on the FLAIR/DWI image acquired at day 1 post-stroke. Lesions were localized individually based on hyperintensity in the image, in addition to an independent radiologist report. Lesions were manually drawn on the image in native space using drawing tools available in FSLview. Registration of each FLAIR/DWI image to the high-resolution structural image was carried out using a linear transformation with 6 degrees-of-freedom. Each high-resolution structural image was registered to the MNI152 template by computing a 12 degree-of-freedom linear affine transformation. The structural-to-standard nonlinear transformation matrices were then applied, using the nearest neighbor interpolation (to avoid 'expansion' of the lesion area), to obtain a registered lesion mask in MNI152 standard space. These standard-space lesion masks were used for further computation of affected and unaffected networks based on a template set of networks. Normally, in the acute phase, DWI images are the most sensitive images for lesion delineation.[29] In our study, images were acquired 24 to 48 hours post-symptoms onset and in most cases, lesions were fully visible in the FLAIR images as well. DWI images were used for first inspection of hyperintensity localization. In the case of a complete match between the hyperintensity evident in the DWI image and the FLAIR image, the FLAIR was used for drawing the mask. In cases where lesions were not fully visible in the FLAIR image ($N = 2$), the mask was drawn on the DWI image. This was done since FLAIR images generally yielded better registration results to MNI152 standard-space.

Eight-Network Template

The eight-network template was taken from Beckmann *et al*[30] (available at: http://www.fmrib.ox.ac.uk/analysis/royalsoc8/). In the current study, the template was used for lesion mapping into affected and unaffected networks, as well as for functional connectivity analysis. Beckmann and colleagues computed a probabilistic independent component analysis[31] using resting-state fMRI data from 10 healthy controls. Probabilistic independent component analysis was used to characterize the spatiotemporal structure of the data. Their results demonstrate high spatial consistency between subjects as well as functional relevance of the revealed networks, which include areas of the visual cortex, sensory and motor systems. Our decision to use this template was based on the functional relevance of the independent components of the template as well as the high consistency across subjects.[30,32] Based on the publication by Beckmann *et al*,[30] the eight-network template can be functionally defined as follows: (a) medial visual cortical areas, (b) lateral visual cortical areas, (c) auditory system, (d) sensorimotor system, (e) visuospatial system (i.e., default-mode network[33]), (f) executive control, (g, h) right and left dorsal visual stream (respectively). For a detailed description of the anatomical structures in each of the networks, see Beckmann *et al*.[30]

To verify that results were not dependent on the choice of network templates, we repeated the analysis using a set of 20 networks from Smith *et al*.[32,34] This analysis yielded similar results to those found for the eight-network template (for further details see Supplementary Material M2, Supplementary Figure S2, and Supplementary Figure S3).

Defining Networks Affected by Lesions

To classify the eight-networks into affected/unaffected individually, an overlap between the binarized eight-networks thresholded template and the individual lesion masks was computed through multiplication. An overlap (minimum of one voxel) resulted in assigning that network as affected; no overlap resulted in assigning that network as unaffected. This yielded a vector of eight networks for each patient. In this vector, values of 0 reflect unaffected network by the individual lesion, and values of 1 reflect affected networks. For a description of lesion sites, see Supplementary Table S1.

Analysis of Functional Connectivity

Functional connectivity maps for each individual functional scan were computed using dual-regression.[35,36] Spatial maps based on a group-ICA of the eight-network template were first used as a set of general linear model regressors on the individual-level. This resulted in a time-course describing the similarity of each volume to the independent component template. These time-courses were then used as general linear model regressors in a second multiple regression analysis, resulting in individual-level spatial maps for each original component. For an example of representative individualized spatial maps see Supplementary Material M3 and Supplementary Figure S4.

To quantify the spatial similarity over time points, we computed the spatial concordance for each patient across time points, such that each component resulted in a single value representing spatial similarity of the network over time. Concordance was computed using concordance correlation coefficient[37] in MATLAB R2011a (The MathWorks Inc., Natick, MA, USA). Concordance values range from 1 (no difference) to -1 (maximal difference). Concordance was computed on thresholded spatial maps using a *z*-value $\geqslant 2.3$ (corresponds to a *p*-value of 0.01). We previously applied a similar approach on the voxel-wise level for exploratory analysis of longitudinal resting-state data from a patient following stroke.[23] The method was extended here to assess changes in concordance at the network level (rather than at the voxel level).

To exclude the lesion area from spatial concordance computation, the individual lesion masks were smoothed (using fslmaths –dilM) and excluded from concordance computation (by means of subtraction from the individual patients maps). This was done to verify that changes in the spatial pattern of functional connectivity maps could not be attributed to changes in the lesion area itself.

To test whether concordance values statistically differed in affected versus unaffected networks, we computed Δ-concordance for each patient: averaging the concordance values for the affected and unaffected networks separately, and then subtracting the averages: $((\mu_{\text{unaffected}}) - (\mu_{\text{affected}}))$. A one-sample *t*-test was used to test for significant difference between concordance in affected and unaffected networks. Figure 1 provides a schematic illustration of the different analysis steps.

Analysis of Clinical Data

In order to investigate the link between changes in functional connectivity as measured by concordance and behavioral change over time, we have used clinical data from day 1 and day 90, as measured by the National Institute of Health Stroke Scale (NIHSS). A measure of Δ-NIHSS was computed and correlated with Δ-concordance by means of Spearman's correlation coefficient. Δ-NIHSS was computed as the ranked absolute difference between the NIHSS obtained at day 1, and the NIHSS obtained at day 90. Higher values thus reflect larger clinical change over time.

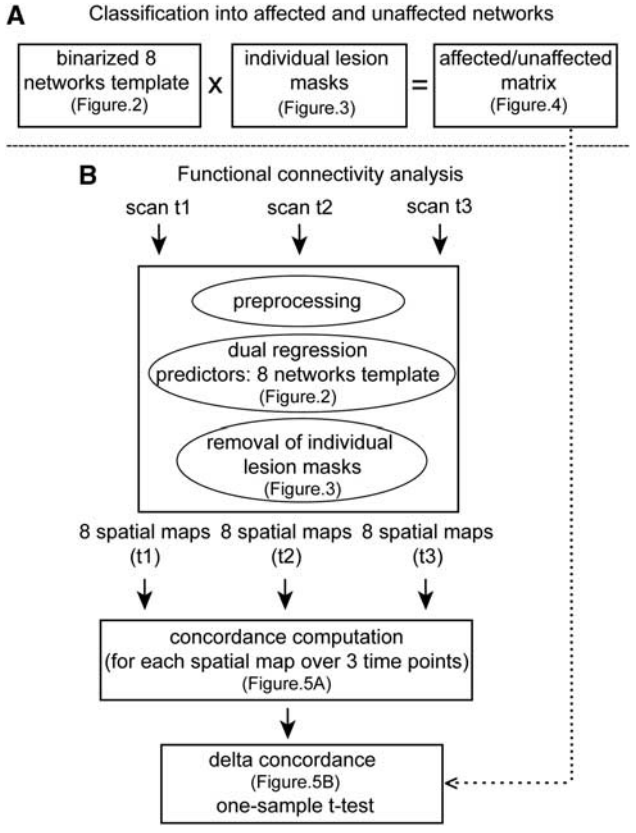

Figure 1. A flow chart of analysis steps. (**A**) Classification of individual lesions into affected and unaffected networks. The binarized eight-network template was multiplied by each individual lesion mask to classify lesions to affected/unaffected matrix. (**B**) Functional connectivity analysis. Each scan was preprocessed and dual-regression was performed. After removal of individual lesion masks, spatial concordance correlation coefficient was computed for each map over three time points. Δ-concordance $((\mu_{\text{unaffected}}) - (\mu_{\text{affected}}))$ was computed and a one-sample *t*-test was performed.

RESULTS

Lesion Mapping: The Network Approach

To map heterogeneous lesions across our sample of patients, we computed the overlap between the eight independent networks (Figure 2) and individual lesions (Figure 3). The overlap result, shown in Figure 4, represents the affected and unaffected networks for each patient's lesion. For example, the lesion for patient 1 was located in the left putamen and left insular cortex. According to the network approach applied here, the networks affected by the lesion were c, d, and f. For patient 2, the lesion was larger in size and was located in the left postcentral gyrus and the left parietal operculum extending into the supramarginal gyrus. The affected networks were networks b–h. For patient 3, the lesion was located in the left pallidum extending to some parts of the left amygdala. Only network c was affected.

The Impact of a Lesion on Functional Connectivity

To explore the influence of a lesion on functional connectivity over time, we computed a measure of spatial concordance of each network, for each patient, across all time points. Figure 5A depicts individual concordance values for each network of each patient. Networks with high concordance values reflect little change over time in the spatial pattern of the functional connectivity maps. After concordance computation, networks were assigned into affected and unaffected as described earlier (see Figure 4). Figure 5B displays the individual Δ-concordance values for each patient. Positive values reflect higher average concordance in unaffected networks, as compared with affected networks. Using a one-sample *t*-test, we found a significant difference ($P = 0.018$, one-sided), indicating that affected networks were significantly less concordant than unaffected networks. This reflects a stronger change in functional connectivity over time in affected networks. We accounted for potential contamination due to changes within the lesion area by excluding it from the analysis.

The Relationship Between Concordance and Clinical Change

To explore the clinical significance of our findings, a correlation between Δ-NIHSS and Δ-concordance was computed using Spearman's correlation coefficient. As alterations in functional connectivity after stroke have been previously shown to correlate with behavior,[9,13,18–20] we hypothesized a positive correlation between the two measures, such that the larger the difference between unaffected and affected networks, the larger the clinical change. As can be seen in Figure 6, a significant ($P = 0.05$, one-sided) positive correlation ($r = 0.5$) was found between the two measures, providing support for the clinical significance of our measure.

DISCUSSION

We found that the changes induced by lesions preferentially impact its functional networks. In order to address this question, we developed a novel analytic approach capable of assessing network-based changes in a heterogeneous stroke population. A generalizable analysis was necessary to investigate whether the effects of localized stroke are relevant to distributed, but interconnected areas, irrespective of the lesion location or implicated

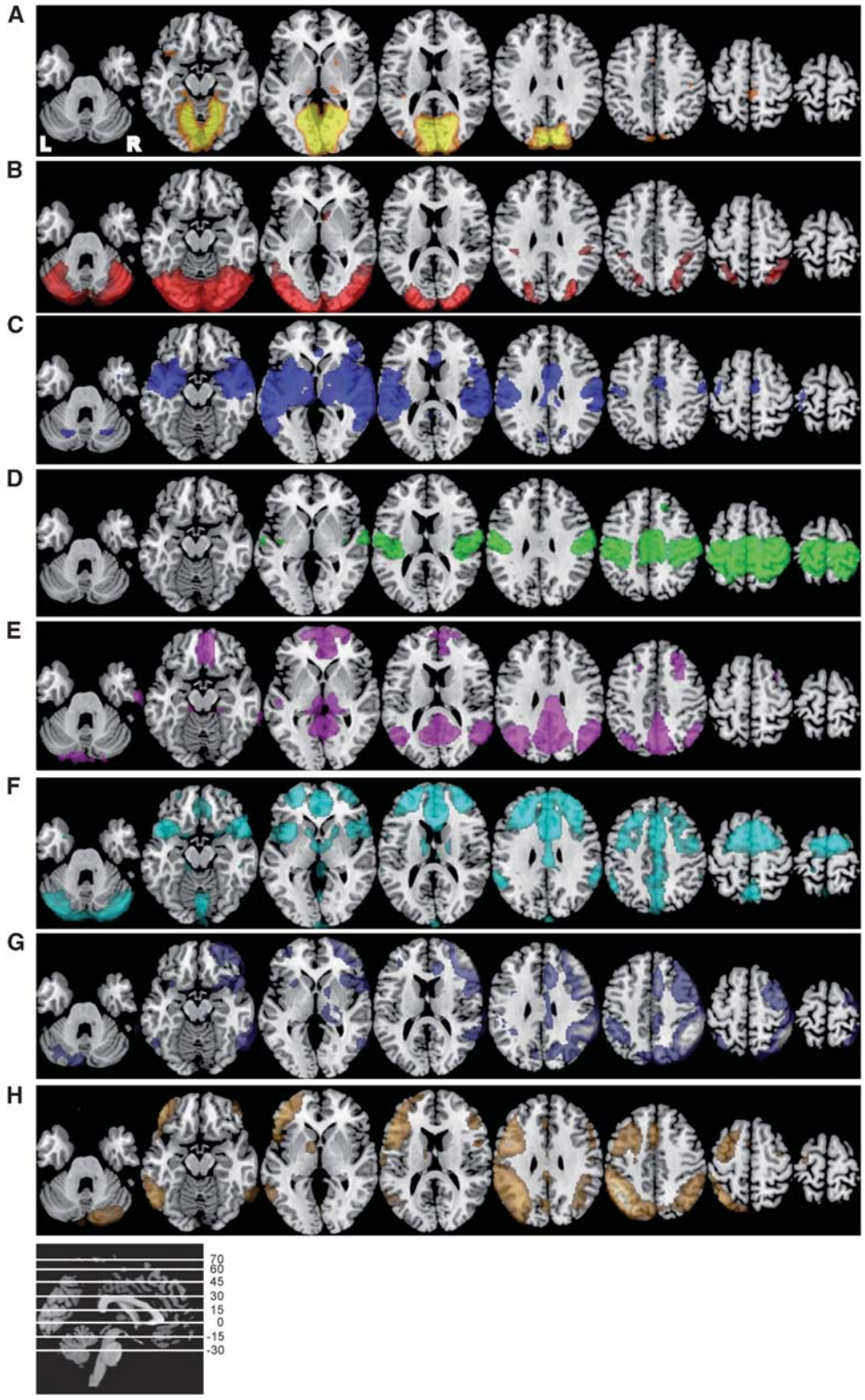

Figure 2. The eight-network template. Axial slices of the eight independent components based on probabilistic independent component analysis in healthy controls ($N = 10$) adopted from Beckmann *et al.*[30] This template was used as a basis for computation of overlap between lesions and networks as well as for dual-regression analysis. Images are shown in neurological convention, *z*-coordinates can be seen on sagittal view. Maps are thresholded based on histogram mixture modeling as described in Beckmann *et al.*

network. Beginning with data acquired 1 day post-stroke onset, we found that networks containing lesions decreased significantly in their concordance over time compared with the unaffected networks. In addition, a significant positive correlation was found between the clinical change over time and alteration in functional connectivity, as measured by Δ-concordance.

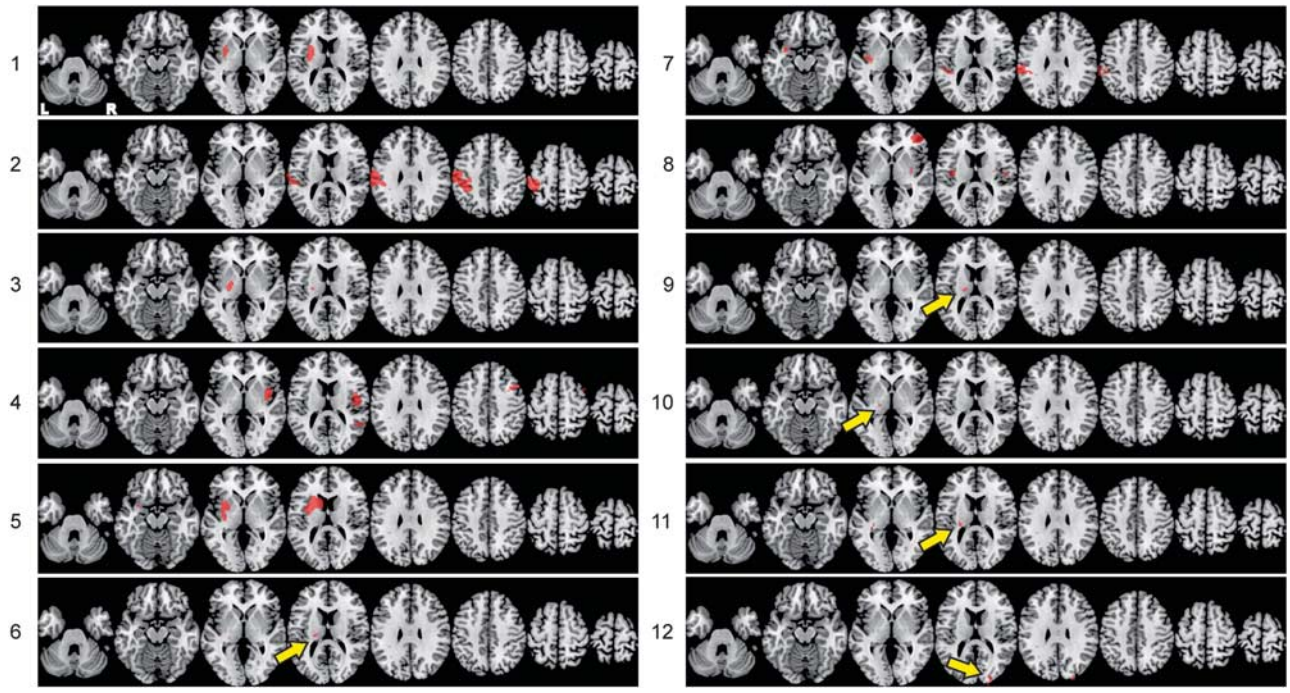

Figure 3. Individualized lesion masks. Axial slices of the individual lesions based on DWI/FLAIR images registered to standard MNI152 space. *z*-coordinates are identical to those presented in Figure 2. Red color depicts areas of hyper-intensity, i.e., the lesioned areas. Yellow arrows are pointing to small lesion areas to improve visibility.

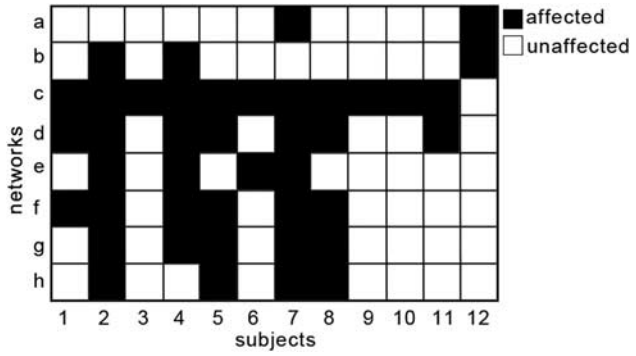

Figure 4. Affected and unaffected networks. Based on the overlap between the eight-network template and the individualized lesion masks, networks were assigned into affected (black) or unaffected (white) for each patient (x-axis). The y-axis depicts individual networks as presented in Figure 2.

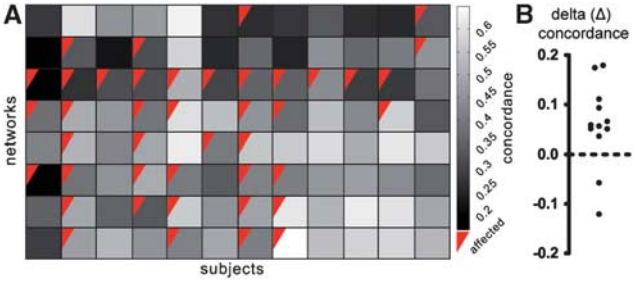

Figure 5. Spatial concordance in affected and unaffected networks. (**A**) Spatial concordance as computed over time for each patient (x-axis) and for each network (y-axis). High values reflect a small change in the spatial pattern. Red triangles depict affected networks. (**B**) Δ-concordance ($(\mu_{\text{unaffected}}) - (\mu_{\text{affected}})$) was computed for each patient demonstrating a significant positive distribution as tested by one-sample *t*-test.

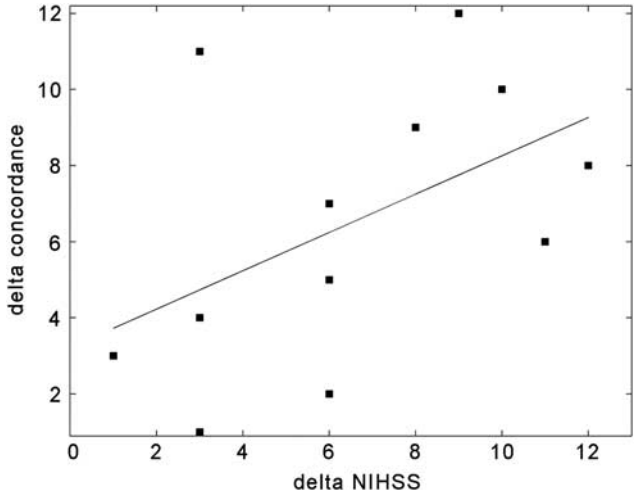

Figure 6. Relationship between Δ-concordance and clinical change. Positive correlation between changes in clinical scores over time as measured by Δ-NIHSS (x-axis) and changes in functional connectivity as measured by Δ-concordance (y-axis). Both axes depict the ranked values (as Spearman's correlation was applied to statistically test the relationship). Black line depicts the fitted regression line.

This correlation provides support for the clinical significance of our findings.

Our results are in line with previous work demonstrating that alterations in functional connectivity after stroke extend beyond the lesion area. For example, He *et al* [9] reported a breakdown of interhemispheric functional connectivity within the attention network in stroke patients with neglect symptoms. Symptom severity correlated with decreased connectivity, and recovery from symptoms correlated with the recovery of normal connectivity patterns. Similar results have been reported in the

sensorimotor[12,13,18,20,38] and language networks.[39] In addition to the well-established correlation between functional connectivity and behavioral symptoms, intervention/treatment has been shown to normalize functional connectivity patterns,[40–42] emphasizing the potential usefulness of functional connectivity as a surrogate measure of functional recovery and for the assessment of rehabilitation tools (for detailed reviews, see Carter *et al*[43] and Grefkes and Fink[44]).

Alterations of functional connectivity in heterogeneous lesions have been previously explored by Nomura *et al*.[11] Patients were examined using a single scan at least 5 months post-stroke or injury. The results demonstrated double dissociation of two cognitive control networks (frontoparietal and cingulo-opercular). Functional connectivity was decreased within the damaged networks more than within the undamaged network. While in Nomura *et al* the network approach was the basis for supporting independence between two networks, our results extend these findings to involve networks falling outside of the lesion area across the whole brain. In addition, Nomura *et al* addressed a chronic stroke population using a single scan, while we were interested in the functional change over time. While Nomura *et al* established the relation between lesions and functional connectivity-based networks, it was our aim to expand such findings to a generalized understanding of changes in network recovery over time.

Owing to the challenge of acquiring longitudinal data in a stroke population, only three studies have addressed the dynamics of functional connectivity during rest after stroke in humans,[13,18,19] all addressing recovery within the motor network. Park and colleagues[18] explored dynamics within the ipsilesional primary motor area and found decreased interhemispheric connectivity, which was most prominent 1-month post-stroke onset. Wang and colleagues[13] used graph theory to describe a gradual shift towards a random graph structure, suggesting a less-effective network state. They explored changes starting at 1-week post-stroke onset. Recently, Golestani and colleagues[19] have addressed the longitudinal recovery after stroke starting the acute phase (<24 hours). They demonstrated decreased interhemispheric connectivity within the motor network at the acute phase, which recovered 7 days post-stroke in recovered patients. Their work is the first longitudinal stroke study beginning in the acute phase. Their results demonstrate the importance of acute resting-state data to capture early changes in functional connectivity and behavioral outcome after stroke.

Experimental stroke research in rats has also demonstrated similar results to those reported in humans.[45–47] Van Meer et al[45] explored the longitudinal effect of unilateral stroke on the sensorimotor system in rats and found decreased interhemispheric and increased intrahemispheric synchronization. Over the course of recovery, reorganization and relative normalization of functional connectivity correlated with behavior.

The measure of concordance presented here reflects a change in functional connectivity and cannot explain directionality or the source of change within a network. One of the potential limitations of concordance is that certain networks are generally more stable over time than others.[23,48] For example, Lohmann *et al*, who proposed the use of voxel-wise concordance with functional connectivity data, found brain areas that were more concordant than others in healthy controls.[23] However, in our analysis, concordance is computed for each subject individually, producing one single value for each network over time. This decreases the potential influence of differences in levels of concordance between subjects. In addition, the fact that our sample is heterogeneous, with lesions distributed across different networks, further reduces the potential confound for within-subject comparison.

The relationship between alterations in functional connectivity after stroke and behavioral outcome/performance has been previously reported for specific networks.[9,13,18–20] In our study, although the clinical significance of our findings should be further explored by examining the link between specific clinical outcome in the different networks (with their respective domains) and concordance, our results support the theoretical framework concerning the influence of a lesion on a complex network of interconnected brain regions. This view is supported as well by the well-known phenomenon of diaschisis[49] in which, after stroke, regions far from the lesion site can show altered metabolic and neural activity. Changes in functional connectivity in general and our suggested approach in particular can be used to shed light on this phenomenon.

The study of longitudinal effects of stroke on functional networks in heterogeneous stroke populations can contribute to our understanding of intrinsic networks organization in the human brain. By providing insight into the recovery process after stroke, future research into large-scale networks may prove valuable for rehabilitation and prognosis.

DISCLOSURE/CONFLICT OF INTEREST

The authors declare no conflict of interest.

ACKNOWLEDGEMENTS

We thank Dr Karsten Müller, Dr Guido Hesselmann, Dr Fatma Imamoglu, and Dr Gabriele Lohmann for their help and advice in various stages of this project.

REFERENCES

1 Sporns O. From simple graphs to the connectome: networks in neuroimaging. *Neuroimage* 2011; **62**: 881–886.
2 Sporns O, Chialvo DR, Kaiser M, Hilgetag CC. Organization, development and function of complex brain networks. *Trends Cogn Sci* 2004; **8**: 418–425.
3 Bullmore E, Sporns O. The economy of brain network organization. *Nat Rev Neurosci* 2012; **13**: 336–349.
4 Bullmore E, Sporns O. Complex brain networks: graph theoretical analysis of structural and functional systems. *Nat Rev Neurosci* 2009; **10**: 186–198.
5 Ovadia-Caro S, Nir Y, Soddu A, Ramot M, Hesselmann G, Vanhaudenhuyse A *et al.* Reduction in inter-hemispheric connectivity in disorders of consiousness. *PLoS ONE* 2012; **7**: e37238.
6 Boly M, Massimini M, Garrido MI, Gosseries O, Noirhomme Q, Laureys S *et al.* Brain connectivity in disorders of consciousness. *Brain Connect* 2012; **2**: 1–10.
7 Buckner RL, Sepulcre J, Talukdar T, Krienen FM, Liu H, Hedden T *et al.* Cortical hubs revealed by intrinsic functional connectivity: mapping, assessment of stability, and relation to Alzheimer's disease. *J Neurosci* 2009; **29**: 1860–1873.
8 Greicius M. Resting-state functional connectivity in neuropsychiatric disorders. *Curr Opin Neurol* 2008; **21**: 424–430.
9 He BJ, Snyder AZ, Vincent JL, Epstein A, Shulman GL, Corbetta M. Breakdown of functional connectivity in frontoparietal networks underlies behavioral deficits in spatial neglect. *Neuron* 2007; **53**: 905–918.
10 He BJ, Shulman GL, Snyder AZ, Corbetta M. The role of impaired neuronal communication in neurological disorders. *Curr Opin Neurol* 2007; **20**: 655–660.
11 Nomura EM, Gratton C, Visser RM, Kayser A, Perez F, D'Esposito M. Double dissociation of two cognitive control networks in patients with focal brain lesions. *Proc Natl Acad Sci USA* 2010; **107**: 12017–12022.
12 Grefkes C, Nowak DA, Eickhoff SB, Dafotakis M, Kust J, Karbe H *et al.* Cortical connectivity after subcortical stroke assessed with functional magnetic resonance imaging. *Ann Neurol* 2008; **63**: 236–246.
13 Wang L, Yu C, Chen H, Qin W, He Y, Fan F *et al.* Dynamic functional reorganization of the motor execution network after stroke. *Brain* 2010; **133**(Pt 4): 1224–1238.
14 Rossini PM, Calautti C, Pauri F, Baron JC. Post-stroke plastic reorganisation in the adult brain. *Lancet Neurol* 2003; **2**: 493–502.
15 Hillis AE, Barker PB, Beauchamp NJ, Gordon B, Wityk RJMR. perfusion imaging reveals regions of hypoperfusion associated with aphasia and neglect. *Neurology* 2000; **55**: 782–788.
16 Hillis AE, Gold L, Kannan V, Cloutman L, Kleinman JT, Newhart M *et al.* Site of the ischemic penumbra as a predictor of potential for recovery of functions. *Neurology* 2008; **71**: 184–189.
17 Feeney DM, Baron JC. Diaschisis. *Stroke* 1986; **17**: 817–830.

18 Park CH, Chang WH, Ohn SH, Kim ST, Bang OY, Pascual-Leone A *et al.* Longitudinal changes of resting-state functional connectivity during motor recovery after stroke. *Stroke* 2011; **42**: 1357–1362.
19 Golestani AM, Tymchuk S, Demchuk A, Goodyear BG. Longitudinal evaluation of resting-state FMRI after acute stroke with hemiparesis. *Neurorehabil Neural Repair* 2013; **27**: 153–163.
20 Carter AR, Astafiev SV, Lang CE, Connor LT, Rengachary J, Strube MJ *et al.* Resting interhemispheric functional magnetic resonance imaging connectivity predicts performance after stroke. *Ann Neurol* 2010; **67**: 365–375.
21 Alstott J, Breakspear M, Hagmann P, Cammoun L, Sporns O. Modeling the impact of lesions in the human brain. *PLoS Comput Biol* 2009; **5**: e1000408.
22 Honey CJ, Sporns O. Dynamical consequences of lesions in cortical networks. *Hum Brain Mapp* 2008; **29**: 802–809.
23 Lohmann G, Ovadia-Caro S, Jungehulsing GJ, Margulies DS, Villringer A, Turner R. Connectivity concordance mapping: a new tool for model-free analysis of FMRI data of the human brain. *Front Syst Neurosci* 2012; **6**: 13.
24 Hotter B, Pittl S, Ebinger M, Oepen G, Jegzentis K, Kudo K *et al.* Prospective study on the mismatch concept in acute stroke patients within the first 24 h after symptom onset—1000Plus study. *BMC Neurol* 2009; **9**: 60.
25 Wahlund LO, Barkhof F, Fazekas F, Bronge L, Augustin M, Sjogren M *et al.* A new rating scale for age-related white matter changes applicable to MRI and CT. *Stroke* 2001; **32**: 1318–1322.
26 Van Dijk KR, Sabuncu MR, Buckner RL. The influence of head motion on intrinsic functional connectivity MRI. *Neuroimage* 2012; **59**: 431–438.
27 Jenkinson M, Bannister P, Brady M, Smith S. Improved optimization for the robust and accurate linear registration and motion correction of brain images. *Neuroimage* 2002; **17**: 825–841.
28 Jenkinson M, Smith S. A global optimisation method for robust affine registration of brain images. *Med Image Anal* 2001; **5**: 143–156.
29 Luby M, Bykowski JL, Schellinger PD, Merino JG, Warach S. Intra- and interrater reliability of ischemic lesion volume measurements on diffusion-weighted, mean transit time and fluid-attenuated inversion recovery MRI. *Stroke* 2006; **37**: 2951–2956.
30 Beckmann CF, DeLuca M, Devlin JT, Smith SM. Investigations into resting-state connectivity using independent component analysis. *Philos Trans R Soc Lond B Biol Sci* 2005; **360**: 1001–1013.
31 Beckmann CF, Smith SM. Probabilistic independent component analysis for functional magnetic resonance imaging. *IEEE Trans Med Imaging* 2004; **23**: 137–152.
32 Laird AR, Fox PM, Eickhoff SB, Turner JA, Ray KL, McKay DR *et al.* Behavioral interpretations of intrinsic connectivity networks. *J Cogn Neurosci* 2011; **23**: 4022–4037.
33 Raichle ME, MacLeod AM, Snyder AZ, Powers WJ, Gusnard DA, Shulman GL. A default mode of brain function. *Proc Natl Acad Sci USA* 2001; **98**: 676–682.
34 Smith SM, Fox PT, Miller KL, Glahn DC, Fox PM, Mackay CE *et al.* Correspondence of the brain's functional architecture during activation and rest. *Proc Natl Acad Sci USA* 2009; **106**: 13040–13045.
35 Beckmann CF, Mackay CE, Filippini N, Smith S. Group comparison of resting-state FMRI data using multi-subject ICA and dual regression. *Fifteenth Annual Meeting of the Organization for Human Brain Mapping* 2009.
36 Filippini N, MacIntosh BJ, Hough MG, Goodwin GM, Frisoni GB, Smith SM *et al.* Distinct patterns of brain activity in young carriers of the APOE-epsilon4 allele. *Proc Natl Acad Sci USA* 2009; **106**: 7209–7214.
37 Lin LI. A concordance correlation coefficient to evaluate reproducibility. *Biometrics* 1989; **45**: 255–268.
38 Carter AR, Patel KR, Astafiev SV, Snyder AZ, Rengachary J, Strube MJ *et al.* Upstream dysfunction of somatomotor functional connectivity after corticospinal damage in stroke. *Neurorehabil Neural Repair* 2012; **26**: 7–19.
39 Warren JE, Crinion JT, Lambon Ralph MA, Wise RJ. Anterior temporal lobe connectivity correlates with functional outcome after aphasic stroke. *Brain* 2009; **132**(Pt 12): 3428–3442.
40 Nowak DA, Grefkes C, Ameli M, Fink GR. Interhemispheric competition after stroke: brain stimulation to enhance recovery of function of the affected hand. *Neurorehabil Neural Repair* 2009; **23**: 641–656.
41 Hummel FC, Cohen LG. Non-invasive brain stimulation: a new strategy to improve neurorehabilitation after stroke? *Lancet Neurol* 2006; **5**: 708–712.
42 Grefkes C, Nowak DA, Wang LE, Dafotakis M, Eickhoff SB, Fink GR. Modulating cortical connectivity in stroke patients by rTMS assessed with fMRI and dynamic causal modeling. *Neuroimage* 2010; **50**: 233–242.
43 Carter AR, Shulman GL, Corbetta M. Why use a connectivity-based approach to study stroke and recovery of function? *Neuroimage* 2012; **62**: 2271–2280.
44 Grefkes C, Fink GR. Reorganization of cerebral networks after stroke: new insights from neuroimaging with connectivity approaches. *Brain* 2011; **134** (Pt 5): 1264–1276.
45 van Meer MP, van der Marel K, Wang K, Otte WM, El Bouazati S, Roeling TA *et al.* Recovery of sensorimotor function after experimental stroke correlates with restoration of resting-state interhemispheric functional connectivity. *J Neurosci* 2010; **30**: 3964–3972.
46 van Meer MP, van der Marel K, Otte WM, Berkelbach van der Sprenkel JW, Dijkhuizen RM. Correspondence between altered functional and structural connectivity in the contralesional sensorimotor cortex after unilateral stroke in rats: a combined resting-state functional MRI and manganese-enhanced MRI study. *J Cereb Blood Flow Metab* 2010; **30**: 1707–1711.
47 van Meer MP, Otte WM, van der Marel K, Nijboer CH, Kavelaars A, van der Sprenkel JW *et al.* Extent of bilateral neuronal network reorganization and functional recovery in relation to stroke severity. *J Neurosci* 2012; **32**: 4495–4507.
48 Shehzad Z, Kelly AM, Reiss PT, Gee DG, Gotimer K, Uddin LQ *et al.* The resting brain: unconstrained yet reliable. *Cereb Cortex.* 2009; **19**: 2209–2229.
49 Finger S, Koehler PJ, Jagella C. The Monakow concept of diaschisis: origins and perspectives. *Arch Neurol* 2004; **61**: 283–288.

Supplementary Information accompanies the paper on the Journal of Cerebral Blood Flow & Metabolism website (http://www.nature.com/jcbfm)